International Journal of Heat and Mass Transfer 74 (2014) 121–127

Contents lists available at ScienceDirect

International Journal of Heat and Mass Transfer

journal homepage: www.elsevier.com/locate/ijhmt

Coupling of temperatures and power outputs in hybrid photovoltaic and thermoelectric modules

Weiqing Lin [a], Tien-Mo Shih [a,b,*], Jin-Cheng Zheng [a,*], Yufeng Zhang [a,*], Jincan Chen [a]

[a] Department of Physics, Xiamen University, Xiamen 361005, China
[b] Institute for Complex Adaptive Matter, University of California, Davis, CA, United States

ARTICLE INFO

Article history:
Received 22 March 2013
Received in revised form 20 August 2013
Accepted 26 February 2014
Available online 1 April 2014

Keywords:
Thermoelectric
Photovoltaic
Hybrid system
Seebeck
Bandgap
Solar-energy conversion

ABSTRACT

The hybrid system of a photovoltaic solar-cell module and a thermoelectric module has drawn considerable attention recently. Here, unlike most of the previously reported work, we present an analysis that intimately couples the nodal temperatures of the system and power outputs of both modules. Within the range of selected solar constants, we have obtained efficiencies for hybrid systems in comparison with those of photovoltaic solar cells alone. Our findings indicate that, for parametric values chosen herein, the former are generally lower than the latter, unless thermal electric materials of low-valued thermal conductivities and high-valued Seebeck coefficients can be found or fabricated.

1. Introduction

Photovoltaic solar cells are devices that convert solar energy into electricity.

During the conversion process, a portion of the impinging radiation is absorbed by the cells, causing the rise of the photovoltaic temperature. It is known [1] that, for photovoltaic cells, the output power decreases as the temperature increases. Therefore, if we are able to design a hybrid system consisting of a solar-cell unit and a thermoelectric module, allowing the latter to dissipate the absorbed energy in the former, and at the same time to reduce the photovoltaic temperature, there may be some hope to produce a larger amount of the output electric power than the solar-cell module alone.

During recent decades, advantages of thermoelectric devices have gradually been realized because these devices are capable of directly converting the thermal energy into the electricity within small sizes. Characteristics of thermoelectric modules alone were investigated [2–4]. In [5], researchers started focusing on heat dissipation of a hybrid system. A couple of years later, van Sark [6] adopted a new type of thermoelectric material when designing the device. A hybrid system with water cooling was also studied [7]. Using heat flux concentrators, Vorobiev et al. [8] developed a hybrid system that yielded high efficiencies. In [9], evacuated-tube heat-pipe solar collectors were studied, with agreeable comparisons of theoretical results and experimental data. A computational study [10] using the finite element method was conducted for a hybrid system with a collector panel inserted between the photovoltaic cell and the thermoelectric module, yielding high thermal efficiencies. Finally, in [11], the thermoelectric module was computationally investigated, with the solar flux input as one of the boundary conditions.

Here in this analysis we have placed the emphasis on the coupling between discretized nodal temperatures in the heat conduction phenomenon and the electrical power outputs produced by the hybrid system. In other words, nodal temperatures are functions of power outputs, and vice versa. Therefore, $T(i)$, P_{te}, and P_{PV} are strongly inter-related. The thermoelectric efficiency, η_{te}, is not assumed to be the maximum value. These variables must be computed simultaneously. Such a coupling approach constitutes a nonlinear challenge, and is presented below.

2. Modeling and formulations

The system schematic of an assembly consisting of a photovoltaic solar unit and a slab of thermoelectric material is shown in Fig. 1. The sunlight impinges upon the top surface of the assembly.

* Corresponding authors. Address: Department of Physics, Xiamen University, Xiamen, China. Tel.: +86 05922184421 (T.-M. Shih).
E-mail addresses: tmshih@xmu.edu.cn (T.-M. Shih), jczheng@xmu.edu.cn (J.-C. Zheng), yufengzhang@xmu.edu.cn (Y. Zhang).

http://dx.doi.org/10.1016/j.ijheatmasstransfer.2014.02.075
0017-9310/

Nomenclature

A_c	area of the hybrid system (m^2)
bi_1	Biot number defined as $h_1\Delta y_{te}/k_{te}$ for bottom face
bi_5	Biot number defined as $h_5\Delta y_g/k_g$ for top face
c	speed of light, 3×10^8(m/s)
d_1, d_2	empirical constants given in Eq. (6)
e	elementary charge 1.6×10^{-19}(C)
E	energy of a solar photon (eV)
E_g	bandgap of silicon material (eV)
h	Planck constant 6.63×10^{-34}(J s)
h_1	heat transfer coefficient for the bottom surface (W/m^2 K)
h_5	heat transfer coefficient for the top surface (W/m^2 K)
I	electrical current in thermoelectric module (A)
I_{pv}	electrical current in the solar cell (A)
k_{te}	thermal conductivity of the thermoelectric module (W/m K)
k_{sub}	thermal conductivity of the substrate in solar cells (W/m K)
k_g	thermal conductivity of the glass layer in solar cells (W/m K)
n	number of p–n pairs in the thermoelectric module
$\dot{N}_E$	$\dot{N}_{gap}$ per unit electron volt
$\dot{N}_{gap}$	number of solar photons per unit time per unit area, carrying energy larger than the bandgap
q_s	heat flow rate entering the control volume (W)
q_n	heat flow rate leaving the control volume (W)
P_j	energy of Joule heating (W)
P_{pv}	power output of photovoltaic solar cells (W)
P_{te}	power output of thermoelectric module (W)
P_{hybrid}	power output of the hybrid system (W)
Rr	radiative recombination rate at zero quasi-Fermi level (same unit as $\dot{N}_{gap}$)
R, r	external and internal resistances of thermoelectric module circuit (Ω)
S	Seebeck coefficient of thermoelectric module (μV/K)
Sc	solar irradiance (solar constant) (W/m^2)
$T_1,\ldots,T_5$	nodal temperatures at node 1,…,5 (K)
T_{air}	temperature of the ambient air (K)
T_{surr}	temperature of the surroundings (K)
V_{te}	voltage of the thermoelectric module circuit (V)
V_{pv}	external voltage of the solar cell (V)
Δy_{te}	half thickness of the thermoelectric module (m)
Δy_{sub}	half thickness of the substrate (m)
Δy_g	half thickness of the glass layer (m)

Greek symbols

α, β	constants related to bandgap and given in Eq. (8)
ε	emissivity of the protective glass layer
ρ	reflectivity of the protective glass layer
σ	Stefan–Boltzmann constant (5.67×10^{-8} W/(m^2 K^4))
η_{hybrid}	efficiency of the hybrid system

A sheet of photovoltaic thin film is imbedded inside the unit filled with the protective glass and the substrate material, respectively, above and below the film. Underneath the solar-cell unit, a thermoelectric module is attached. Both of the bottom surface and the top surface of the assembly are cooled by air flows.

The system is assumed to be in steady state, and the heat transfer phenomenon takes place in the one-dimensional manner, with all variables being functions of the y coordinate only. Based on the first law of thermodynamics, we can derive five nonlinear algebraic equations governing T_1, T_2, T_3, T_4, and T_5, as shown in Fig. 1. Even though we are aware that heat fluxes flow downward in real-life situations, we will proceed to assume that they flow upward along the positive y direction to avoid sign confusions.

For T_1,

$$A_c h_1 (T_{air} - T_1) = A_c k_{te}(T_1 - T_2)/\Delta y_{te} + P_{te}(1), \tag{1}$$

which can be simplified and rearranged, with final coefficients listed in Table 1. The power output, $P_{te}(1)$, can be expressed by

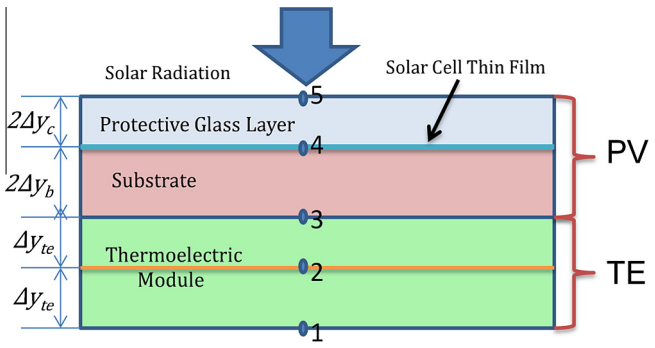

Fig. 1. The system schematic representing the hybrid system of photovoltaic solar cell and thermoelectric module.

$$P_{te}(1) = V(1)I - P_j(1), \tag{2a}$$

in which the Seebeck electrical current, I, is needed. The relationship between the current and the Seebeck voltage can be expressed by

$$I = (V(1) + V(2) + V(3))/(R + r(1) + r(2) + r(3)), \tag{2b}$$

$$P_j(1) = I^2 r(1), \tag{2c}$$

$$\text{where} \quad V(1) = \text{nS}(T_{1.5} - T_1), \quad T_{1.5} = (T_1 + T_2)/2, \tag{2d}$$

$$\text{and} \quad r(1) = e_1(r_0 + \beta T_1). \tag{2e}$$

Values of e_1, r_0, and β are given in Appendix A. Definitions of voltages, internal electrical resistance, and midpoint nodal temperatures at other nodes can also be found in Appendix A. The constant n is the number of p–n semi-conductor pairs, and S is the Seebeck coefficient. It can be observed that, via Eqs. (1, 2a–e), the electrical current and the nodal temperatures are strongly coupled.

For the derivation of the governing equation for T_2, the control volume, over which the energy conservation is taken, is shown in the dashed line in Fig. 2. The nodal temperature T_2 is situated at the center of the control volume. From south, the heat flux enters the control volume. It leaves the control volume to north. The Joule heating can be treated as a heat sink inside the control volume, and does not explicitly appear in the energy-conservation equation. In addition, there is power output due to Seebeck thermoelectric effects. These quantities are designated, respectively, as q_s, q_n, and P_{te}. Consequently, according to the flux directions indicated by arrows, we obtain

$$q_s - q_n - P_{te}(2) = 0, \tag{3}$$

where

$q_s = A_c k_{te}(T_1 - T_2)/\Delta y_{te}$, and $q_n = A_c k_{te}(T_2 - T_3)/\Delta y_{te}$.

Table 1
The matrix coefficients for the nonlinear set of 5 equations governing nodal temperatures, power output of the thermoelectric module, and power output of the photovoltaic solar cell, along with the constant vector.

$$\mathrm{a}=\begin{bmatrix} -1-bi_1 & 1 & 0 & 0 & 0 \\ 1 & -2 & 1 & 0 & 0 \\ 0 & -k_{te}/\Delta y_{te} & -k_{te}/\Delta y_{te}-k_{sub}/\Delta y_{sub} & k_{sub}/\Delta y_{sub} & 0 \\ 0 & 0 & k_{sub}/\Delta y_{sub} & -k_{sub}/\Delta y_{sub}-k_g/\Delta y_g & k_g/\Delta y_g \\ 0 & 0 & 0 & 1 & -1-bi_5 \end{bmatrix}$$

$$\mathrm{b}=\begin{bmatrix} P_{te}(1)\Delta y_{te}/(k_{te}A_c)-bi_1T_{air} \\ P_{te}(2)\Delta y_{te}/(k_{te}A_c) \\ P_{te}(3)/A_c \\ P_{pv}/A_c \\ \left[-S_c+\in\sigma\left(T_5^4-T_{surr}^4\right)+\rho S_c\right]\Delta y_g/k_g-bi_5T_{air} \end{bmatrix}$$

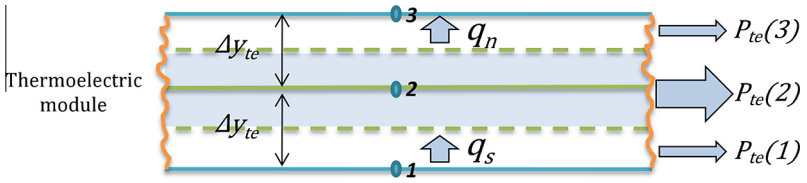

Fig. 2. A typical control volume containing nodal temperature, T_2. It is noted that P_j and P_{te} should bear the same sign.

The thermoelectric power output, $P_{te}(2)$, can be obtained in a similar manner as Eq. (2a).

In the derivation of the governing equation for T_3, which is located at the interface between the thermoelectric material and the photovoltaic module, we idealize the thermal contact resistance to be zero. After straightforward algebraic manipulations, we obtain

$$a(3,2)T_2+a(3,3)T_3+a(3,4)T_4=b(3), \tag{4}$$

where the coefficients are listed in Table 1.

The derivation of the governing equation for T_4 is similar to that for T_3. The final equation can also be cast into the standard form as

$$a(4,3)T_3+a(4,4)T_4+a(4,5)T_5=b(4). \tag{5}$$

It is worth noting that the electrical power delivered by the photovoltaic film can be related to the nodal temperature by

$$P_{pv}=A_c(d_1+d_2T_4), \tag{6}$$

where $d_1$and d_2 are constants, whose values depend on the impinging solar constants, and can be computed *a priori* independently of the system characteristics. Such a linear approximation greatly simplifies the analysis, enabling us to officially couple the nodal temperatures and the power outputs.

The details are briefly given below.

First, the number of solar photons per unit time per unit area, carrying energy (that is larger than the bandgap) per electron volt can be given as

$$\dot{N}_E=(AM1.5)(hc/E^3), \tag{7}$$

where $AM1.5$ stands for NREL's (National Renewable Energy Laboratory) data for the solar spectrum at $Sc=1000\ \mathrm{W/m^2}$, with its unit being $\mathrm{W/m^2\,nm}$; h represents the Planck constant, 6.63×10^{-34} J s; the symbol, c, is the speed of light, 3×10^8 m/s.

Next, according to [12], the bandgap, E_g, decreases with increasing temperatures, and can be written as

$$E_g(T)=E_g(0)-\alpha T^2/(T+\beta), \tag{8}$$

where $E_g(0)=1.1557$ eV, $\alpha=7.021\times10^{-4}$ eV/K, and $\beta=1108$ K.

Only photons that carry the energies greater than the bandgap are capable of exciting the electrons located in the valence band, and force them to jump to the conduction band. The number of such photons can be expressed by

$$\dot{N}_{gap}=\int_{E_g}^{\infty}\dot{N}_E dE=\int_{E_g}^{\infty}(AM1.5)\left(\frac{hc}{E^3}\right)dE=\text{function of } T. \tag{9}$$

A portion of the excited electrons may return to the valence band, and recombine with holes. For such recombination activities, the rate can be derived as

$$Rr=\frac{2\pi}{c^2h^3}\int_{E_g}^{\infty}\frac{E^2dE}{exp[E/(k_BT)]-1}, \tag{10}$$

thus inviting Eq. (8) to enter the problem [13]. The electrical current is generated from the electron–hole pairs that do not recombine. Note that the only recombination mechanism considered in this analysis is caused by radiation. Under this idealization, we can write

$$I_{pv}=e\dot{N}_{gap}-eRr\{exp[eV_{pv}/(k_BT)]-1\}, \tag{11}$$

where the internal series resistance and the shunt resistance of solar cells have been neglected. Finally, the output power of the solar cell can be expressed by

$$P_{pv}=V_{pv}I_{pv}=\text{function of } V_{pv}. \tag{12}$$

Under the assumption that solar cells deliver the maximum power output, we can numerically find the corresponding maximum power output from Eq. (12). The laborious procedure of finding d_1 and d_2 can be briefly described as (a) give a value of T; (b) compute

Table 2
Constant values of d_1 and d_2 for various values of Sc.

Sc(W/m^2)	d_1	d_2
800	440.070	−0.579
1000	510.337	−0.592
2000	1064.852	−1.287
3000	1532.460	−1.661
4000	2043.820	−2.173
5000	2555.176	−2.677
6000	3066.575	−3.173

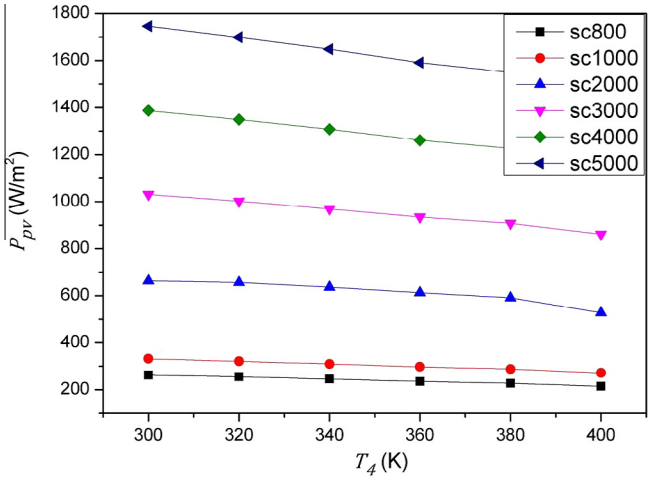

Fig. 3. Power output of photovoltaic solar cell versus the temperature of the thin-film solar cell, parametrized in solar constants.

E_g according to Eq. (8); (c) find maximum P_{pv}; finally (d) use the curve fitting to obtain d_1 and d_2. Table 2 lists their values for Sc = 800–6000 W/m^2.

In Fig. 3, a family of nearly linear lines of P_{pv} versus the photovoltaic temperature are plotted, parameterized in six various values of Sc for silicon solar cells. Finally, it is also noted that we assume the film to be so thin like a sheet (of a few nanometers) that its thickness is negligible in comparison with those of thermoelectric module, the substrate, and the protective glass layer.

For the derivation of the governing equation for T_5, we take the energy balance over the half-grid-interval control volume between $x_{4.5}$ (the average of x_4 and x_5 and the top surface. This balance dictates that the northbound heat conduction due to the temperature gradient between node 4 and node 5 should be equal to the energy leaving the sheet (thus, energy components entering the sheet should be considered negative), eventually yielding

$$T_4 - (1 + bi_5)T_5 = c_5 \Delta y_{sub}/k_{sub}, \tag{13}$$

where c_5 includes energy components of radiation and convection entering and exiting above the top surface, and is defined as

$$c_5 = q_{r,net} + (\rho - 1)Sc - h_5 T_{air}. \tag{14}$$

In Eq. (14), the first term denotes the net radiation loss from the system to the surroundings, and is written as

$$q_{r,net} = \in \sigma\left(T_5^4 - T_{surr}^4\right). \tag{15}$$

Equation (15) holds under the assumption that the area of the absorbing top surface of the hybrid system is much smaller than that of the surroundings, such as the sky. In the present analysis, this assumption is certainly valid. In addition, it should be made clear that the temperature of the surroundings, such as clouds in the sky, may not necessarily be the same as that of the ambient air near the earth ground.

Equations (1), (2a)–(2e), (3)–(15) constitute a set of nonlinear equations governing the characteristics of the assembly system. When the solution converges, the efficiency of the hybrid system can be defined and computed by

$$\eta_{hybrid} = P_{hybrid}/Sc = [P_{te}(1) + P_{te}(2) + P_{te}(3) + P_{pv}]/Sc. \tag{16}$$

The solution procedure is described in the next section.

3. Computational procedure

Equations (1), (2a)–(2e), (3)–(16) can be solved using the standard Newton–Raphson (NR) method [14]. However, we are concerned that, after interspersing linearized terms (related to photovoltaic and thermoelectric behaviors) with linear terms discretized from the heat conduction, we may encounter difficulties in debugging the code in the event of divergences. Therefore, we have opted the adoption of a modified version of NR method, in which two stages of computations are conducted. In the first stage, nonlinear terms are left in the right-hand side of equations. For the sake of convergence safety, the linearized solution obtained by using a direct linear solver is preferably under-relaxed. In the second stage, all nonlinear terms are computed using the newly iterated and under-relaxed values. The procedure then repeats.

It is understood that this two-staged under-relaxed NR version is clearly not as robust as the standard NR version, and its convergence rate is also slower than the standard NR counterpart. The advantage of this modified version, however, is twofold: (1) a great amount of labor associated with algebraic manipulations and coding is saved, and (2) debugging the code is easier when divergence happens. Regardless of choices, the two solutions computed using these two methods should become identical upon solution convergence. The concept of this mathematical modeling is similar to that of the compartment modeling widely used in ecological sciences [15].

Fig. 4 shows the flow chart of the computer code. In the first stage, nodal temperatures are computed iteratively, with power outputs of the hybrid system either guessed or previously iterated. Iterations are needed because the radiation term, T^4, exists in Eqs. (13)–(15). In the second stage, these more accurate nodal temperatures are used to update values of internal electrical resistances in

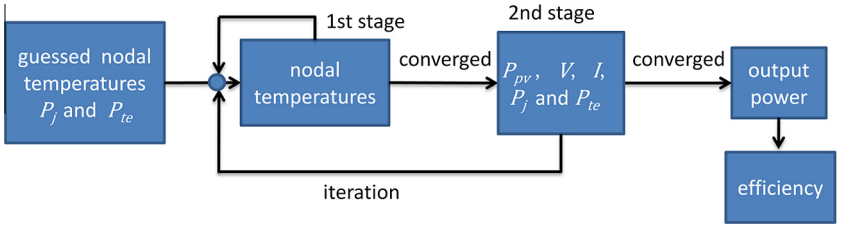

Fig. 4. Flowchart of the algorithm that is used to iteratively compute nodal temperatures, power output of the thermoelectric module, and power output of the photovoltaic solar cell.

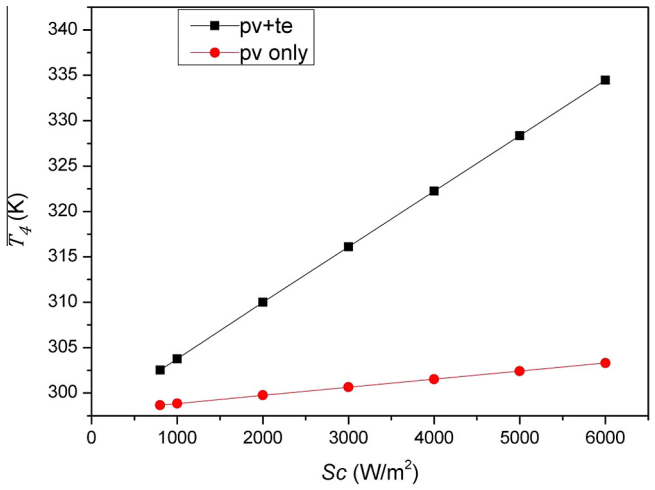

Fig. 5. Comparison of the temperature of the thin-film solar cell for two cases: (a) photovoltaic solar cell only, and (b) the hybrid system.

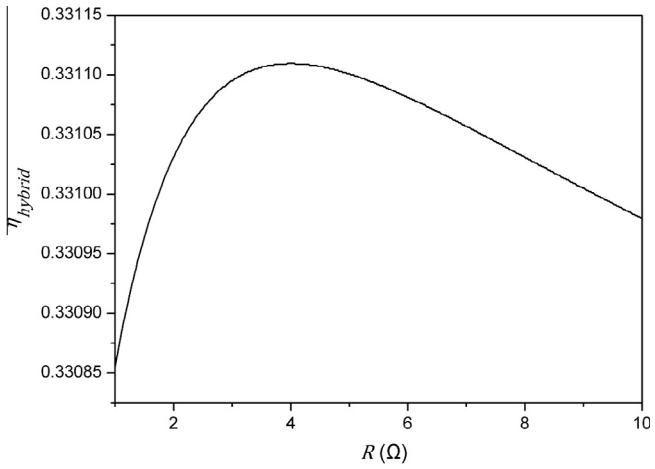

Fig. 6. Efficiency versus external electrical resistance. The R value that corresponds to the maximum efficiency is chosen for computations.

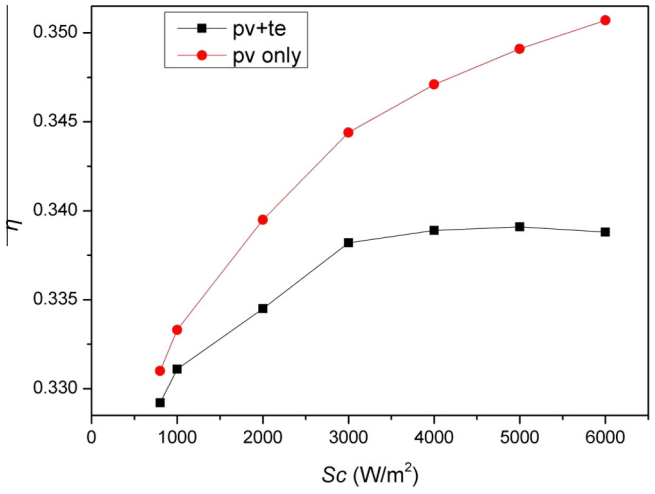

Fig. 7. Comparison of efficiencies for two cases: (a) photovoltaic solar cell only ($\eta = P_{pv}/Sc$), and (b) the hybrid system.

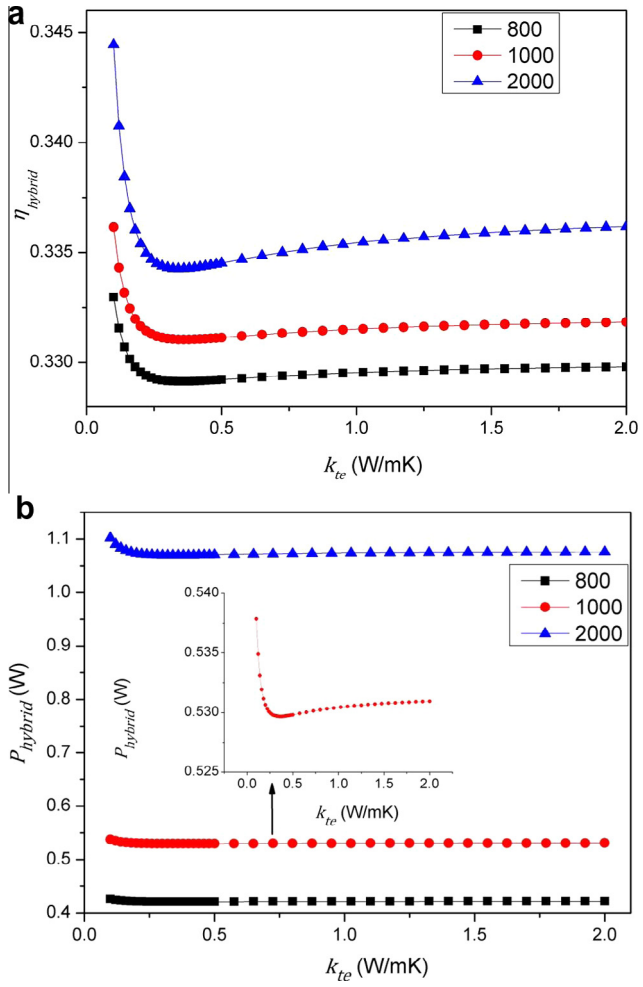

Fig. 8. (a) Efficiency of the hybrid system versus the thermoelectric thermal conductivity, and (b) power output of the hybrid system versus the thermoelectric thermal conductivity. Both cases are parametrized in *Sc*.

the thermoelectric module and these power outputs. For all runs, the global energy balance has been checked to ensure the correctness of the code.

4. Results and discussion

Fig. 5 shows the photovoltaic temperature, T_4, versus the solar constant, *Sc* for both cases of (a) the photovoltaic thin film only and (b) the hybrid assembly of photovoltaic thin film and thermoelectric module. Both temperatures are almost linear functions of *Sc*. They are, however, associated with different slopes. It is observed that values of the hybrid case are overall higher than those of the thin film case, suggesting that the addition of the thermoelectric module blocks the cooling effect. As *Sc* increases, the difference in two temperatures also increases.

To choose an appropriate value of external electrical resistance, *R*, we have first evaluated the efficiencies of the hybrid system corresponding to various values of given *R*. Then the value that yields the maximum efficiency is chosen, as shown in Fig. 6. For example, for a typical run with the following data:

$Sc = 1000$ W/m^2, $k_{te} = 0.48$ W/(m K), $n = 100$, $L_{te} = 0.003$ m, $L_{sub} = 0.003$ m, $L_{glass} = 0.003$ m, r = 3.9973 Ω (computed), and $R = 3.9925$ Ω,

the efficiency of the hybrid system is equal to 0.3311.

In Fig. 7, we present the efficiency, η, versus the solar constant, Sc for both cases of (a) the photovoltaic thin film only and (b) the PV–TE hybrid assembly. Both curves exhibit the trend that the efficiency increases as the solar constant increases as expected. Within the range of the investigated Sc values, the efficiency of the hybrid system is lower than that of the photovoltaic solar cell alone. This finding offers a warning guide for the industrial manufacturers who may be interested in fabricating such hybrid systems, with the hope that the hybrid systems will yield higher efficiencies.

Finally, Fig. 8a and b depict the efficiency, η_{hybrid} and the combined power output, P_{hybrid} versus the thermal conductivity of thermoelectric module, k_{te}. We note that both η_{hybrid} and P_{hybrid} decrease as k increases for $k_{te} \leqslant 0.25$. Beyond this k_{te} value, both the efficiency and the power output remain fairly unchanged. Another noteworthy feature is that the sensitivity of η_{hybrid} on k_{te} is quite high within the range of low k_{te} values. If thermoelectric materials having low k_{te} values can, indeed, be fabricated, it appears possible for the industry to design a hybrid system that is capable of yielding high values of thermal efficiencies.

With the advances on thermoelectric research, such as the enhancement of power factor (electrical conductivity times square of Seebeck coefficient) through optimizing transport distribution functions [16] or nanostructure designs [17,18], and the reduction of thermal conductivity by nanostructure scattering [17,19] or strain engineering [20], the efficiency of thermoelectric energy conversion can be greatly increased. The PV–TE hybrid system can thus be potentially advantageous due to such significant improvements of thermoelectric materials.

It is worth mentioning as a tender reminder that, in our analysis, the power output of the solar-cell module is approximated by a linear function of the solar-cell temperature, with constants, d_1 and d_2, comprehensively computed according to Eqs. (7)–(12). The benefit of this approximation is that the power output is reliably coupled with the nodal temperatures of the PV–TE hybrid system.

5. Conclusions

In this study, we have emphasized on coupling the temperature field with the power outputs of the hybrid system that consists of a photovoltaic solar-cell module and a thermoelectric module. The efficiency of the thermoelectric module is directly computed based on thermoelectric theories, and the value of the external electrical resistance is taken to be the one corresponding to the maximum value of efficiency. Primary findings can be summarized below:

1. According to our findings within the parametric values chosen, the thermal efficiency of the hybrid system is generally lower than that of the solar-cell module alone. If we are able to fabricate thermoelectric materials with low-valued thermal conductivities and high-valued Seebeck coefficients, it may be possible for us to achieve $\eta_{hybrid} > \eta_{pv\ only}$.
2. The power output of the solar cell module can be approximated *a priori* by a linear function of the temperature $T(4)$, which is then coupled with other nodal temperatures. Such an approximation greatly facilitates the thermal analysis.
3. A numerical procedure has been developed to couple the power outputs of both the photovoltaic solar-cell module and the thermoelectric module with the temperature distribution of the hybrid system. It serves as a tool for the future research in designing PV–TE hybrid assemblies.

Conflict of Interest

All authors hold absolutely no conflict of interest toward this submitted paper, if published.

Acknowledgments

This work is supported by the Specialized Research Fund for the Doctoral Program of Higher Education (Grant 20120121110021), Natural Science Foundation of China (Grant U1232110), Natural Science Foundation of Fujian Province of China (Grant 2013J01026), Fundamental Research Funds for Central Universities (Grant 2013121012), and Institute for Complex Adaptive Matter, University of California, Davis, CA 95616 (Grant ICAM-UCD13-08291).

Appendix A

e_1	2.5×10^4	
e_2	5.0×10^4	
e_3	2.5×10^4	
r_0	$1.0 \times 10^{-5}\ \Omega$	
β	$1.0 \times 10^{-7}\ \Omega/K$	
$r(1)$	$e_1(r_0+\beta T_1)$	internal electrical resistance
$V(1)$	$nS(T_{1.5}-T_1)$	voltage
$T_{1.5}$	$(T_1+T_2)/2$	midpoint nodal temperature
$r(2)$	$e_2(r_0+\beta T_1)$	internal electrical resistance
$V(2)$	$nS(T_{2.5}-T_{1.5})$	voltage
$T_{2.5}$	$(T_2+T_3)/2$	midpoint nodal temperature
$r(3)$	$e_3(r_0+\beta T_1)$	internal electrical resistance
$V(3)$	$nS(T_3-T_{2.5})$	voltage

References

[1] D. Faiman, S.M. Tuladhar, J.M. Kroon, M.M. Wienk, T. Fromherz, F. Padinger, C.J. Brabec, N.S. Sariciftci, Temperature dependence for the photovoltaic device parameters of polymer–fullerene solar cells under operating conditions, J. Appl. Phys. 90 (10) (2001) 5343–5350.
[2] G.J. Snyder, E.S. Toberer, Complex thermoelectric materials, Nat. Mater. 7 (2008) 105–114.
[3] D. Kraemer, B. Poudel, H.P. Feng, J. Christopher Caylor, B. Yu, X. Yan, Y. Ma, X.W. Wang, D.Z. Wang, A. Muto, K.M. Enaney, M. Chiesa, Z.F. Ren, G. Chen, High-performance flat-panel solar thermoelectric generators with high thermal concentration, Nat. Mater. 10 (2011) 532–538.
[4] J.C. Zheng, Recent advances on thermoelectric materials, Front. Phys. China 3 (3) (2008) 269–279.
[5] H.Y. Yu, Y.Q. Li, Y.H. Shang, B. Su, Experiment investigation and optimization on photovoltaic–thermoelectric hybrid power source, Acta Energiae Sol. Sinica 30 (4) (2009) 436–440.
[6] W.G.J.H.M. van Sark, Feasibility of photovoltaic–thermoelectric hybrid modules, Appl. Energy 88 (8) (2011) 2785–2790.
[7] D.J. Yang, H.M. Yin, Energy conversion efficiency of a novel hybrid solar system for photovoltaic, thermoelectric, and heat utilization, IEEE Trans. Energy Convers. 26 (2) (2011) 662–670.
[8] Y. Vorobiev, J. González-Hernández, P. Vorobiev, L. Bulat, Thermal–photovoltaic solar hybrid system for efficient solar energy conversion, Sol. Energy 80 (2006) 170–176.
[9] W. He, Y.H. Su, Y.Q. Wang, S.B. Riffat, J. Ji, A study on incorporation of thermoelectric modules with evacuated-tube-heat-pipe solar collectors, Renew. Energy 37 (2012) 142–149.
[10] Y. Deng, W. Zhu, Y. Wang, Y.M. Shi, Enhanced performance of solar-driven photovoltaic–thermoelectric hybrid system in an integrated design, Sol. Energy 88 (2013) 182–191.
[11] P. Li, L.L. Cai, P.C. Zhai, X.F. Tang, Q.J. Zhang, M. NIINO, Design of a concentration solar thermoelectric generator, J. Electron. Mater. 39 (9) (2010) 1522–1530.
[12] P. Singh, N.M. Ravindra, Temperature dependence of solar cell performance – an analysis, Sol. Energy Mater. Sol. C. 101 (2012) 36–45.
[13] G.D. Wei, K.-T. Shiu, N.C. Giebink, S.R. Forrest, Thermodynamic limits of quantum photovoltaic cell efficiency, Appl. Phys. Lett. 91 (2007) 223507.
[14] T.M. Shih, Numerical Heat Transfer, Springer-Verlag, New York, 1984, pp. 129–130.
[15] J.H.M. Thornley, J. France, Mathematical Models in Agriculture; Quantitative Methods for the Plat, Animal, and Ecological Sciences, Cromwell Press, Trowbridge, UK, 2007.
[16] Z.Y. Fan, H.Q. Wang, J.C. Zheng, Searching for the best thermoelectrics through the optimization of transport distribution function, J. Appl. Phys. 109 (7) (2011) 073713–073716.

[17] Z.Y. Fan, J.S. Zheng, H.Q. Wang, J.C. Zheng, Enhanced thermoelectric performance in three-dimensional superlattice of topological insulator thin films, Nanoscale Res. Lett. 7 (2012) 570–577.
[18] J.Q. He, J.R. Sootsman, L.Q. Xu, S.N. Girard, J.C. Zheng, M.G. Kanatzidis, V.P. Dravid, Anomalous electronic transport in dual-nanostructured lead telluride, J. Am. Chem. Soc. 133 (23) (2011) 8786–8789.
[19] J.Q. He, S.N. Girard, J.C. Zheng, L.D. Zhao, M.G. Kanatzidis, V.P. Dravid, Strong phonon scattering by layer structured $PbSnS_2$ in PbTe based thermoelectric materials, Adv. Mater. 24 (32) (2012) 4440–4444.
[20] N. Wei, L.Q. Xu, H.Q. Wang, J.C. Zheng, Strain engineering of thermal conductivity in graphene sheets and nanoribbons: a demonstration of magic flexibility, Nanotechnology 22 (2011) 105705–105714.